Aalborg Universitet

AALBORG UNIVERSITY
DENMARK

A Monopole-Based Wideband Absorber for Ultra Large Angles

Cai, Yang; Mei, Peng; Chen, Zhi; Lin, Xian Qi; Zhang, Shuai

A Monopole-Based Wideband Absorber for Ultra Large Angles

Yang Cai, *Student Member, IEEE*, Peng Mei, *Member, IEEE*, Zhi Chen, Xian Qi Lin, *Senior Member, IEEE,* and Shuai Zhang, *Senior Member, IEEE*

Abstract—**This paper develops a broadband absorber by fully using the radiation features of monopole antennas for ultrawide-angle absorption application. A unit cell (UC) based on monopole antennas is proposed, and its working polarization is analyzed with the antenna reciprocity method (ARM) and image theory. A wide-angle impedance matching (WAIM) layer is also introduced to further enhance the absorption at large angles. The optimized monopole-based UC reveals 90% absorptivity from 5.5 to 14.76 GHz at the incident angle of 80°. To the best of our knowledge, this is the first time to report an absorber that can work perfectly under such ultrawide angles in a broadband manner. An 11 × 36 array is configured and simulated to verify the effectiveness of the monopole-based UC. The monostatic and bistatic scattering are both reduced significantly as well as other diffuse scattering directions from the simulated results. A prototype of 110 mm × 360 mm is fabricated and measured. Time gating methods are adopted to diminish the direct coupling effect. The measurements are in good agreement with the full-wave simulation results.**

Index Terms—**Absorber, broadband, large incident angle, antenna reciprocity, scattering cross-section (SCS) reduction, time gating.**

I. INTRODUCTION

Electromagnetic (EM) absorbers have been developing for many decades. They are widely used in anechoic chambers [1], and co-designed with antennas for multiple functions [2]–[4]. Profile, bandwidth, polarization, and angular stability are four fundamental merits of an absorber. Great efforts are devoted into the former three properties [5]–[7]. Researches for angular stability are still in demand. Most of the literature on large-angle absorption suffers from narrow bandwidth especially at shadow incidence, i.e., incident angles approaching horizontal plane. Conventional broadband absorbers maintain a stable frequency response up to 30-40° oblique angles, and some may reach 60° or 70° with a limited

band [8]–[16]. Those ultra-wide-angle absorbers usually work at resonances, leading to a narrow band or multiple narrow bands. Designing a broadband absorber for ultra-large oblique incidence (e.g. around 80° oblique angles) are still challenging. Recently some literature sheds light on that [17]–[19]. Nevertheless, measurement under such ultra-large angles brings further difficulties. The direct coupling between transmitting and receiving antennas and desired reflection from absorbers becomes intertwined as oblique angle increases. Even time-gating method will be inapplicable then.

Some structures are designed especially for large incident scenarios, such as oblique-flat-sheets [17] and folded resistive patches [18]. Simulated results suggest good performance, but measurements under normal incidence are merely given in [17], [18]. The characteristic mode (CM) analysis is employed in [19], in which a broadband absorption is achieved within 82° oblique incidence for transverse magnetic (TM) polarization and 45° for transverse electric (TE) one.

In the aforementioned literature on absorbers for large angles, the surface current distribution is always illustrated and analyzed to interpret the absorbing principle but without a generalized designing procedure. In this paper, a novel broadband absorber for ultra-large-angle absorption is proposed using antenna reciprocity. Referring to the antenna reciprocity method [20], [21], we design a monopole-structured broadband absorber for ultra-large-angle absorption. Furthermore, a wide-angle impedance matching (WAIM) layer, which is widely used in phased array antennas to enhance the scanning performance [22], [23], is designed to further enhance the absorption performance.

Simulation results of the proposed monopole-based absorber UC achieve 90% absorptivity from 5.5 to 14.76 GHz at the incident angle of 80° under TM polarization and maintain 80% absorptivity at 85°. An 11 × 36 absorbers array is then configured to observe the bistatic SCS results, which suggests a significant reduction at the specular direction compared to the same size metal ground plane. The total reflection power in the space is decreased dramatically as well. Although the designed absorber works merely at ultra large angles, it provides a novel approach to cope with the dilemma of bandwidth and large angles. Furthermore, referring to the proposed method, broadband absorption at full-angles could be achieved by properly selecting structures, such as combining the monopole structure with a conventional small-angle absorber.

This article is organized as follows. In Section II, the antenna

reciprocity method (ARM) to design absorbers, monopole polarization properties, and blind angles are discussed. In Section III, a monopole structure is designed and the input impedance is studied. WAIM layer is then introduced into the design to improve the performance at large angles. The full-wave simulation is also investigated to demonstrate the effectiveness of the proposed monopole structure, and the bistatic scattering is observed to reveal the reduction of the scattered field intuitively. Measurements of the monopole-based absorber are detailed in Section IV. Conclusions and further discussion are presented in Section V.

II. CONCEPT

A. Antenna reciprocity and array theory

Antenna reciprocity states that the receiving and transmitting properties (e.g., bandwidth, radiation pattern) of an antenna are identical. This principle is firstly introduced and applied in the design of absorbers in [20], where an antenna is regarded as an absorber when it operates at the receiving mode and the port is terminated with proper lumped elements (e.g., resistor, capacitor, or inductor). On the other hand, radiation patterns are taken into consideration in [21]. Antennas can radiate and receive EM waves in the same pattern according to the antenna reciprocity. Incident waves from the maximum radiating direction are thus well received and absorbed when matching loads are terminated. The conventional dipole-based absorbers work in the broadside patterns resembling a horizontal dipole or patch antenna, where the maximum radiation is at broadside as shown in Fig. 1(a), indicating that the receiving performance at broadside direction is the best among all incident angles, and the poor performance at large angles as shown in Fig. 1(b). Perfect reception is therefore expected for a vertical monopole antenna at ultra large angles because of its conical radiation pattern as illustrated in Fig. 1(c).

Except for the antenna mode as discussed above, the residual mode or structural mode contributes to the scatter of an antenna as well. The concept is introduced in [24], where the conclusion that an minimum scattering antenna (MSA) with a ground plane can achieve significant reduction in scattering if it's conjugate matched is drawn. In that case, the residual mode can be neglected as the ground plane is no larger than the antenna.

According to the aforementioned concept, an absorber with ultra large angle absorption performance is designed by using monopole antennas due to its unique radiation features. Typically, a monopole antenna above an infinite metal ground radiates like isolated vertical dipoles of double length, which radiates at small grazing angles, i.e., angles approaching the horizon. According to the antenna reciprocity, the monopole-based absorber is therefore capable of achieving EM absorption at ultra large incident angles.

Besides, based on the array theory, for transmitting antenna arrays, phase differences are imposed among the antenna elements to steer the main beam. When arrays are operating as receiving mode, signals from the desired direction can be detected, owing to the vector composition, at the output port of the array. Although signals from nulls which are caused by
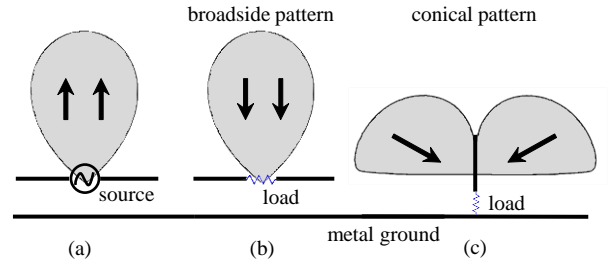

Fig. 1 (a) Radiation and (b) absorption patterns of a horizontal dipole antenna, and (c) absorption pattern of a vertical monopole antenna.

array factors rather than element patterns can not be detected, they are still received and dissipated by the elements provided the terminals of each element are matched and isolated, and scattering effects are thus insignificant. In the case of absorbing arrays, all elements are loaded with proper lumped elements resulting in the fact that the absorbing pattern is determined by the radiating pattern of the UC in the absorbing array. This is the major difference between array radiation patterns and absorbing patterns.

B. Polarization and blind angles

Polarization insensitivity is often preferred for absorbers, which is closely related to the specific structure of an absorber. As is known to all, a good absorption indicates a good impedance match between the absorber and free space However, the reflection coefficient of an absorber for TE and TM oblique incidence waves are quite different, which are described in [25]

$$\Gamma(\text{TE}) = \frac{Z_{\text{in}} - Z_0 / \cos(\theta)}{Z_{\text{in}} + Z_0 / \cos(\theta)}, \tag{1}$$

$$\Gamma(\text{TM}) = \frac{Z_{\text{in}} - Z_0 \times \cos(\theta)}{Z_{\text{in}} + Z_0 \times \cos(\theta)}, \tag{2}$$

where Z_{in} and Z_0 are the input impedance of the absorber and the characteristic impedance of free space, respectively. θ is the incident angle with respect to the normal direction. Generally speaking, as the incident angle increases, the absorption performance of TM polarization deteriorates slowly with the operating band shifting to higher frequencies, while, for TE polarization, the absorption performance suffers severer degradations with its operating band merely shifting. Therefore, it seems impossible to achieve ultrawide-angle absorption for both TE and TM oblique incidence waves.

Alternatively, it can also be explained according to antenna theory. For vertical and horizontal infinitesimal electric dipoles that are positioned above a conducting plane, according to the image theory [26], the virtual sources of horizontal dipoles have 180° polarity difference with respect to the actual sources, while the vertical dipoles' imaginary sources share the same polarity with the real ones. As the incident angle θ increases from 0° to 90°, the electric field, for TM polarization, varies from the horizontal direction to the vertical one, while it remains horizontal for TE polarization. On account of the polarity differences, radiating far filed near the horizon plane

are canceled for TE polarization but reinforced for TM one, in which case EM waves of TE polarization cannot be radiated or received at large angles according to antenna reciprocity. As a result, the working polarization is theoretically limited to TM polarization for large incident angles given the ground plane is perfect electric conductor (PEC). The TE polarization under large incident angles, however, can be absorbed if the ground plane is perfect magnetic conductor (PMC) according to the image theory.

This phenomenon is observed in literature and we can not find one with electric ground achieving perfect absorption under more than 70° TE polarized oblique incidence. The TE polarization under large incident angles, however, can be absorbed if the ground plane is PMC according to the image theory. Since we focus on shadow incidence, TM polarization will mainly be discussed in the rest of this paper.

III. Implementation of the Monopole-Based Absorber

A. Design of the unit cell

In this section, a monopole antenna is firstly designed and its input impedance at specific oblique angles is mainly concerned. As discussed in part A of Section II, if the port is terminated with matching lumped elements, an antenna can absorb the EM waves from the directions that are consistent with the main beam of the monopole antenna.

The proposed monopole UC is illustrated in Fig. 2. This structure is derived from the conventional conical monopole antenna which radiates similarly in different elevation planes owing to its axial symmetry. The metal solid structure is then reduced into three orthodontia planar structures to lighten the weight of the whole structure but remains symmetric in elevation planes. The design procedure is concluded into three steps. The first step is to design a single substrate monopole structure (S1 as shown in Fig. 3). It then develops into symmetric structure with two substrates (S2 as plotted in Fig. 2 (c)). Thereafter we integrate a WAIM layer into S2 to get S3 as shown in Fig. 2 (a).

The configuration of the UC S1 is shown in Fig. 3, where a substrate is perpendicular to the ground plane and a fan-shaped patch is etched on one side of the substrate, connecting to the ground through a lumped port. The image theory is adopted to obtain an effective vertical dipole whose main lobes are close to the horizontal direction.

The fan shape is designed to lower the profile and broaden the impedance bandwidth of the monopole antenna. The master-slave periodical boundary condition (PBC) is applied to the opposite faces of the UC to simulate it in an infinite array environment in Ansys HFSS. When the monopole antenna is simulated as an antenna, the top of the UC is covered with a perfectly matched layer (PML), and the lumped port is assigned to obtain the input impedance as shown in Fig. 3(a). In contrast, when the monopole antenna is simulated as an absorber as shown in Fig. 3(b), the top of the UC is assigned as the Floquet port, and the lumped port is replaced by a lumped resistor. The oblique incident angle θ and polarization angle φ of the incident waves are shown in Fig. 3. The simulated input impedance of
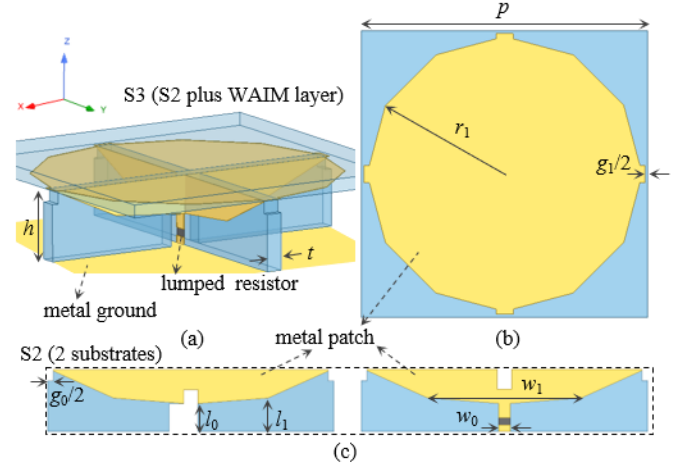

Fig. 2 Geometry of the monopole-based absorber. (a) perspective view of S3 (b) upper WAIM layer. (c) side view of S2.
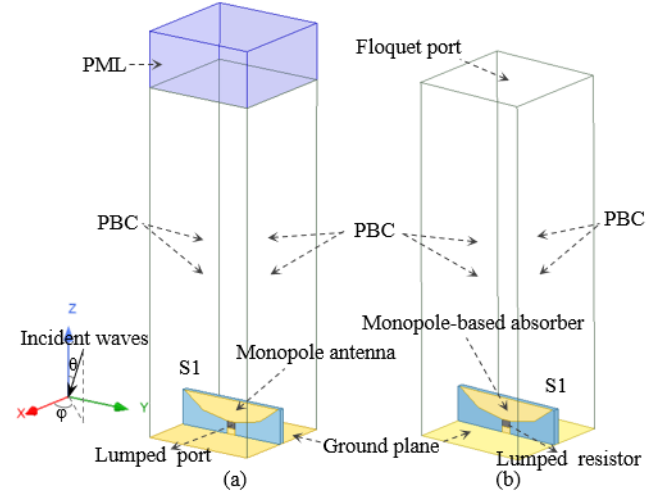

Fig. 3 Simulating configurations for the UC. (a) as an antenna. (b) as an absorber.

the monopole antenna under 80° oblique incidence is plotted in Fig. 4 (red line with squares) where the imaginary part is around zero and the real part is increasing slowly within a wide band. The input impedance of this monopole antenna is almost purely resistive, indicating that it can be matched to a single lumped resistor in a wide band.

Based on the input impedance of the structure S1, the real part is varying from 80Ω to 110Ω, and the corresponding monopole-based absorber is then simulated by simply terminating the port of the monopole antenna with a lumped resistor, where 100Ω is selected as an initial value to achieve the conjugate matching. The reflection coefficient of the monopole-based absorber under 80° oblique incidence is plotted in Fig. 5 (red line with squares), where the absorbing peak is highly consistent with the matching point in Fig. 4.

The absorption of this structure for different azimuth angles varies due to the asymmetry around the z-axis. Another fan shape is therefore added perpendicularly to both the ground plane and the existing substrate, as depicted in Fig. 2(c), to enhance the absorption insensitivity on azimuth planes. The input impedance of the monopole antenna (S2) is plotted in
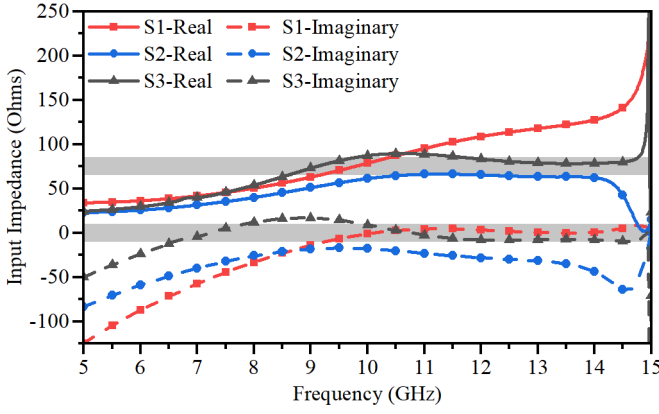
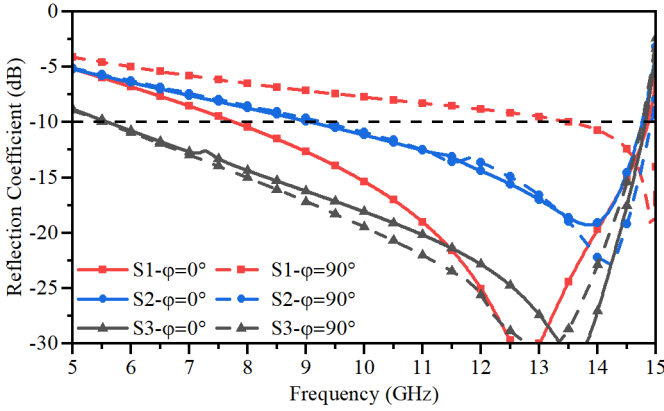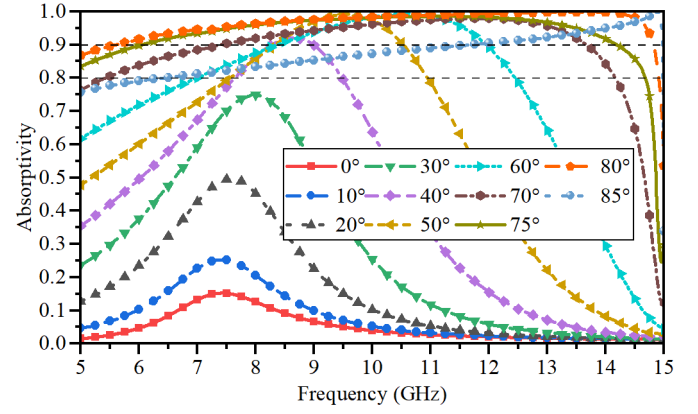Fig. 4 Input impedance of three absorbers under 80° oblique incidence.

Fig. 5 Simulated reflection coefficient of three absorbers under 80° oblique incidence in two polarization planes (φ = 0°, 90°).

(a)

(b)

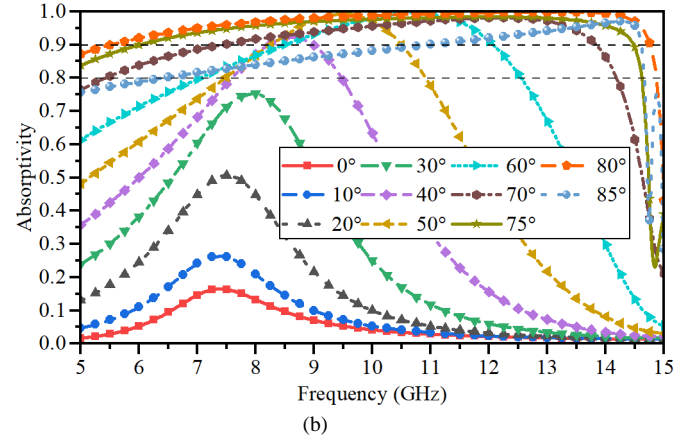Fig. 6 Simulated absorptivity at different incident angles in in two polarization planes (a) φ = 0°, (b) φ = 90°.

Fig. 4 (blue line with circles), where it is observed that the real part of the input impedance decreases from 130 Ω to 70 Ω, and the imaginary part drops a little compared to that of the UC S1.

After reassigning the value of the lumped resistor of S2 as 70Ω, the reflection coefficient in two polarization planes (φ = 0°, 90°) is almost the same as presented in Fig. 5 (blue line with circles). Nevertheless, the reflection coefficient of the UC S2 is deteriorated owing to the mismatch caused by the dropping imaginary part of the input impedance, which can be improved later by a third patch serving as the WAIM layer. The outline of the two substrates is modified and two slots are cut out on each substrate to facilitate the assembling of two monopoles as shown in Fig. 2(c).

In the design of phased antenna arrays, WAIM layers are often utilized to improve the performance of wide-angle scanning. A dodecagon patch is capped above the UC S2 serving as the WAIM layer as illustrated in Fig. 2(b). The four squares at tips are designed to enhance the coupling between two UCs. The coupling can be analyzed through the equivalent circuit [27]. The patch introduces extra inductance and compensates for the imaginary part of the input impedance of absorber with WAIM. With the presence of the WAIM layer, the impedance match improves greatly. As presented in Fig. 4 (shadow block area), the real and imaginary parts are very stable within broadband. The real one is around 75Ω from 8.5GHz to 14.7GHz and the imaginary part is near zero from 6.5GHz to 14.9GHz. The value of the lumped resistor of S3 is

initially set to be 80 Ω. Using the aforementioned procedure, the reflection coefficient of the monopole-based absorber S3 with WAIM layer is obtained as displayed in Fig. 5 (dark grey line with triangles). It can be seen that the lowest operating frequency shifts from 9 GHz to 5.5 GHz with the loading of the WAIM layer. Thereafter, the absorptivity under different incident angles is simulated as shown in Fig. 6, from which we can find that the proposed absorber S3 can work up to 85° with more than 80% absorptivity from 6.45 to 14.66 GHz, and achieve 90% absorptivity around 80° from 5.5 to 14.76 GHz. The total height of the monopole-based absorber is only $0.048\lambda_0$ (corresponding to the free space wavelength at 5.5 GHz). The optimized dimensions of the monopole-based absorber are h = 2.2 mm, t = 0.5 mm, p = 10 mm, r_1 = 4.9 mm, l_0 = 1mm, l_1 = 1.2 mm, w_0 = 0.4mm, w_1 = 5.4 mm, g_0 = 0.8 mm, g_1 = 0.2mm.

B. Design of the absorber array

In order to demonstrate the effectiveness of the proposed absorber with ultrawide-angle absorption, the bistatic scattering cross-section (SCS) of the absorber is simulated. On account of the ultrawide absorbing angle, the scale of the array needs to be large enough so that its main beam can be steered to an ultrawide angle. For the sake of convenience, a rectangular array with a scale of 11 × 36 UCs, as shown in Fig. 7, is designed to enable large-angle scanning along the long side. This configuration can scan a broader angle than a square array with 20 × 20 UCs which has almost the same area. Since UCs
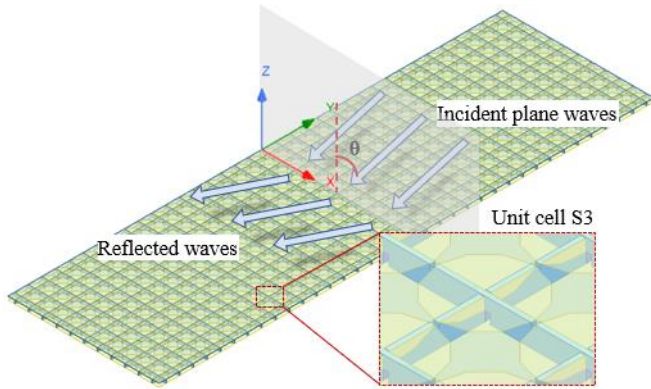
Fig. 7 Configurations for the absorber array.

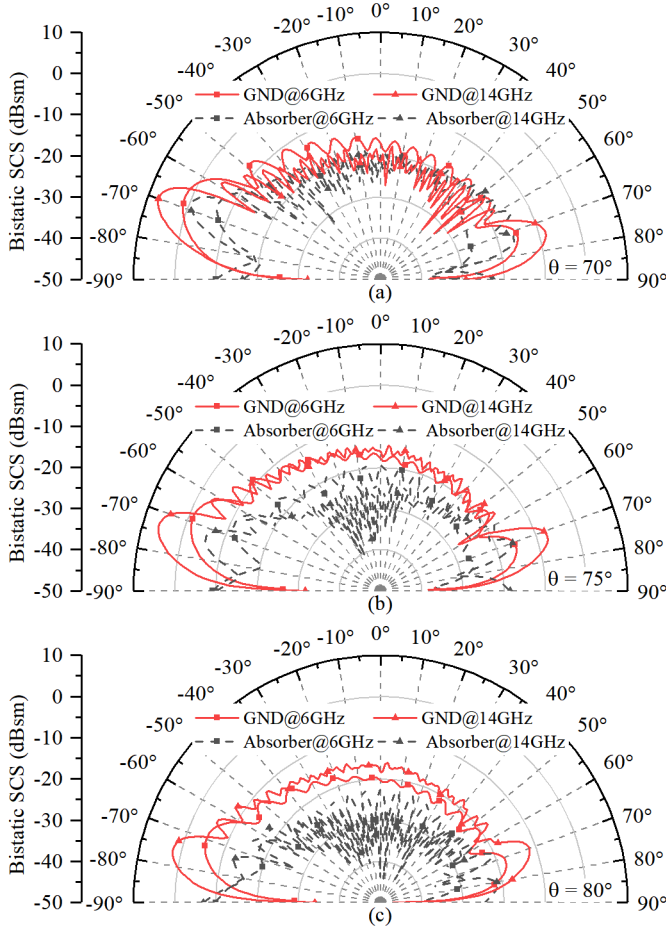Fig. 8 The bistatic SCS of the ground plane and monopole-based absorber in the cutting plane of φ = 90°.

Fig. 9 The comparison of bistatic SCS of the ground plane and monopole array in U-V plane.

work similarly in both planes (φ=0°, 90°), the plane of φ = 90° is chosen to observe the bistatic SCS. For comparison, the bistatic SCS of a metal ground with the same size is also simulated to conclude the SCS reduction of the monopole-based absorber with ultrawide-angle absorption performance.

Plane-wave illuminations are assigned to simulate incident plane waves, and PMLs are set to the outer boundaries. The bistatic SCS in the yoz cutting plane at 70-, 75-, 80-degree incident angles are plotted in Fig. 8. The frequencies of 6 GHz and 14 GHz are selected to elaborate on the SCS reduction and the influence of electrical size on the maximum scan angles,
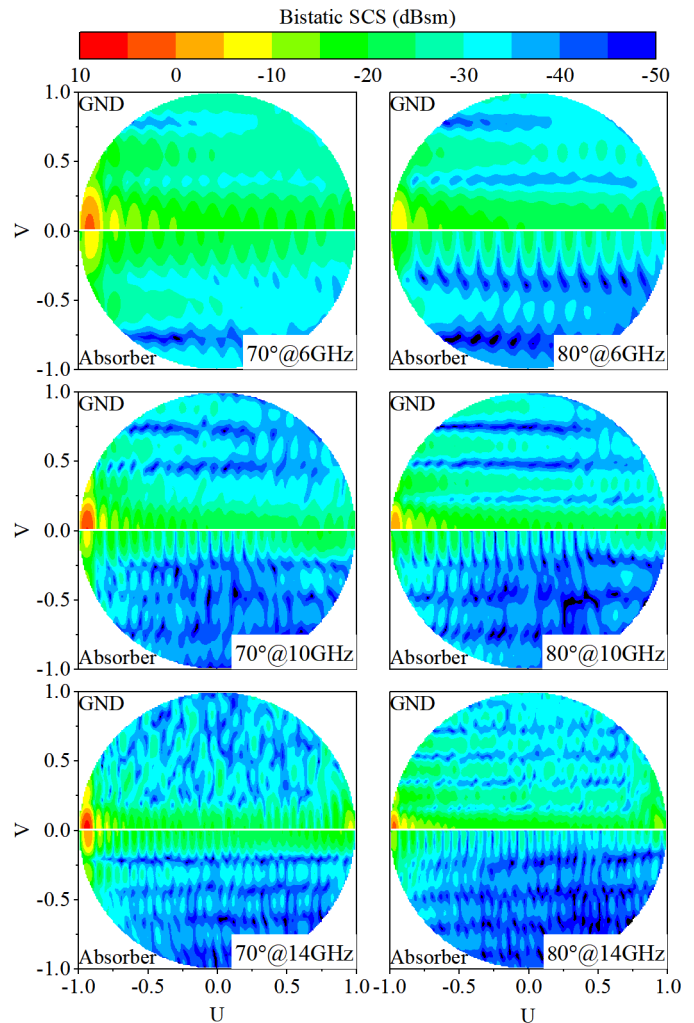
since higher frequency leads to larger electrical size for the same array, and hence larger scan angles. Full-wave simulation results suggest that the bistatic SCS of the monopole-based absorber at the specular reflecting directions are dramatically reduced compared to that of the metal ground. Moreover, the monostatic scattering of the absorber is also reduced significantly compared to that of the metal ground.

For a more intuitive demonstration, the bistatic SCS in the upper space is observed and presented in the U-V plane as displayed in Fig. 9. In each subplot, the upper and lower semi-sphere represents the SCS of the ground plane and monopole-based absorber, respectively. Owing to the symmetry of the structure, half of the upper U-V plane could reveal the scattering feature, hence the bistatic SCS of the metal ground and the monopole-based absorber are put together for a better comparison. It is obvious that the SCS of the proposed absorber is reduced dramatically in specular and diffuse directions compared to that of the metal ground. In addition, the bistatic SCS reduction in terms of the specular direction under different incident angles within a wideband is plotted in Fig. 12 (line with symbols).
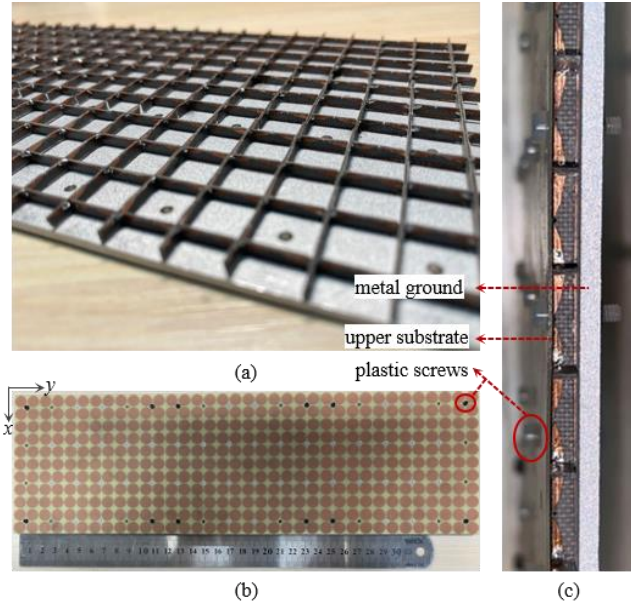
Fig. 10 Photo of the fabricated monopole-based absorber. (a) perspective view without WAIM layer. (b) top view. (c) side view.
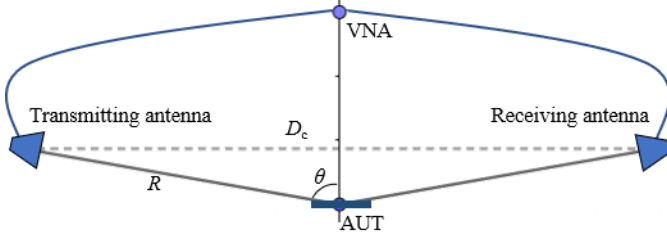

Fig. 11 Setup of the measurement.

IV. FABRICATION AND MEASUREMENT OF THE MONOPOLE-BASED ABSORBER ARRAY

The proposed monopole-based absorber is composed of three substrates, two vertical orthodontia ones, and an upper horizontal one as displayed in Fig. 10 (a) and (b). The substrate of the vertical two and the upper one is F4B with the thickness of 0.5 mm ($\varepsilon_r = 2.65$, $\tan\delta = 0.002$) and FR4 with the thickness of 0.4 mm ($\varepsilon_r = 4.4$, $\tan\delta = 0.02$), respectively. They are assembled onto a metal ground with plastic screws and slots in the ground plane as illustrated in Fig. 10(c). An 11 × 36 monopole-based absorber is fabricated with a total size of 110 mm × 360 mm.

This prototype is measured using an arch-setup as displayed in Fig. 11. To calibrate the measurement, a metal plate with the same shape and area is used as the reference to the prototype. The transmitting and receiving antennas are both linearly polarized horn antennas working from 2 GHz to 18 GHz and tilted away from the normal direction symmetrically to measure the specular bistatic SCS. As the bistatic angle increases, the direct coupling between the transmitting and receiving antennas becomes strong, leading to the degradations of the measured results of the monopole-based absorber. The time gating method is therefore utilized to cope with this problem. The large bistatic angle, however, brings another issue that the coupling and reflective signals are in close vicinity to each other in the time domain if the absorber under test (AUT) is
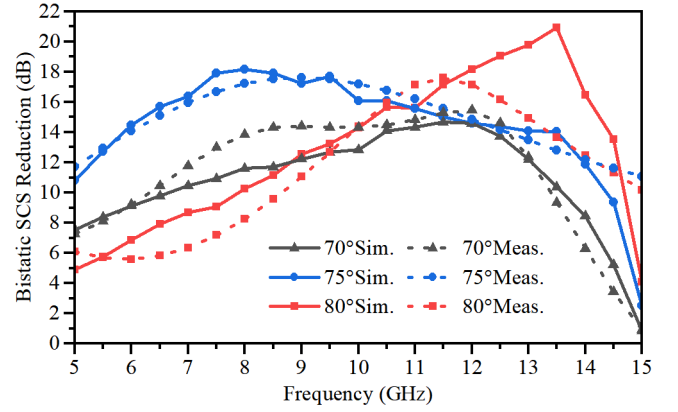

Fig. 12 Comparison of bistatic SCS of the simulated and measured monopole-based absorber.

placed near the transmitting and receiving antennas. As illustrated in Fig. 11, the path difference can be very subtle when incident angle θ is large, and the time difference (t_d) is calculated by

$$t_d = \frac{2R\text{-}D_c}{c} = \frac{2R\left(1\text{-}\sin(\theta)\right)}{c}, \tag{3}$$

where R is the distance between the AUT and transmitting or receiving antennas, D_c is the direct coupling path, θ is the bistatic angle, and c is the speed of light.

When R is 5 m, the corresponding time difference is 0.507 ns, which is fair to distinguish the coupling and reflective signals in this case. After applying the time gating, the measured bistatic SCS reduction of the monopole-based absorber at 70°, 75°, and 80° is plotted in Fig. 12. The measured and simulated results of bistatic SCS reduction agree pretty well with each other. At ultrawide angles (e.g., 80°), the bistatic SCS reduction is around 6 dB at 6.0 GHz that is poor compared to the counterparts at high frequencies, which is mainly due to the relatively small size of the prototype at 6.0 GHz. A comparison of the absorber proposed in the paper and in the literature is listed in TABLE I. Thickness, fractional bandwidth (FBW), and maximum absorbing angles under TM polarization are considered here. The proposed absorber achieves wide-band absorption under ultra-large incident angles with a very low profile.

TABLE I
COMPARISON BETWEEN ABSORBERS

Ref.	Thickness (λ_0)	Bandwidth (GHz) / FBW (%)	Max. Angle under TM
[10]	0.007	4.19, 6.64, 9.95 / <1.5%	45° (90%)
[12]	0.262	5-37 / 152.38%	45° (90%)
[14]	0.022	16.6, 24.4 / <2%	70° (90%)
[15]	0.042	4.2-9 / 72.73%	60° (90%)
[18]	0.096	3.6-11.4 / 104%	75° (90%)
[19]	0.139	1.9-4.2 / 75%	82° (90%)
This Work	**0.048**	**5.5-14.76 / 91.42%** **6.45-14.66 / 77.78%**	**80° (90%)** **85° (80%)**

λ_0: wave length corresponding to the lowest frequency of absorption.

V. Conclusion

In summary, a monopole-based absorber with ultra-large absorbing angles and wide operating bandwidth is described in this article. The antenna reciprocity method (ARM) is adopted to design a monopole-based UC, which can radiate at large angles as an antenna, thereby absorbing EM waves as terminated with matched loads. In addition, a WAIM layer is loaded to cooperate with the monopole-based absorber to enhance its bandwidth. The proposed absorber reveals broadband absorptivity from 70° to 85°, where 90% absorptivity at 80° from 5.5 GHz to 14.76 GHz and 80% absorptivity at 85° from 6.45 GHz to 14.66 GHz are achieved. Based on the large angle properties, a 110 mm × 360 mm monopole-based absorber is then proposed to demonstrate the SCS reduction in the long-side direction. The U-V planes are observed to draw the conclusion that the scattered energy in specular and diffuse directions are dramatically decreased compared to that of an identically sized metal plane. The fabricated prototype suggests great agreement with simulation ones. This paper opens a design space for solutions in broadband and ultra-large oblique incidence absorption, which was always a challenge in the past. The methodology proposed in this paper is brand new and very effective. The proposed antenna reciprocity method can be further applied into other structures to achieve full-angles absorption in the future.

References

[1] C. L. Holloway, R. R. DeLyser, R. F. German, P. McKenna, and M. Kanda, "Comparison of electromagnetic absorber used in anechoic and semi-anechoic chambers for emissions and immunity testing of digital devices," *IEEE Trans. Electromagn. Compat.*, vol. 39, no. 1, pp. 33–47, 1997.

[2] J. Wu, Y. Qi, W. Yu, L. Liu, and F. Li, "An Absorber-Integrated Taper Slot Antenna," *IEEE Trans. Electromagn. Compat.*, vol. 59, no. 6, pp. 1741–1747, Dec. 2017.

[3] P. Mei, X. Q. Lin, J. W. Yu, P. C. Zhang, and A. Boukarkar, "A Low Radar Cross Section and Low Profile Antenna Co-Designed With Absorbent Frequency Selective Radome," *IEEE Trans. Antennas Propag.*, vol. 66, no. 1, pp. 409–413, Jan. 2018.

[4] Z. Shen, J. Wang, and B. Li, "3-D Frequency Selective Rasorber: Concept, Analysis, and Design," *IEEE Trans. Microw. Theory Tech.*, vol. 64, no. 10, pp. 3087–3096, Oct. 2016.

[5] T. J. Prince, E. J. Riley, and S. W. Miller, "Additive Manufacturing of PLA-Based Microwave Circuit-Analog Absorbers," *IEEE Trans. Electromagn. Compat.*, vol. 63, no. 5, pp. 1341–1346, Oct. 2021.

[6] Y. Han, W. Che, C. Christopoulos, and Y. Chang, "Investigation of Thin and Broadband Capacitive Surface-Based Absorber by the Impedance Analysis Method," *IEEE Trans. Electromagn. Compat.*, vol. 57, no. 1, pp. 22–26, Feb. 2015.

[7] S. Sambhav, J. Ghosh, and A. K. Singh, "Ultra-Wideband Polarization Insensitive Thin Absorber Based on Resistive Concentric Circular Rings," *IEEE Trans. Electromagn. Compat.*, vol. 63, no. 5, pp. 1333–1340, Oct. 2021.

[8] Y. Han, W. Che, C. Christopoulos, Y. Xiong, and Y. Chang, "A Fast and Efficient Design Method for Circuit Analog Absorbers Consisting of Resistive Square-Loop Arrays," *IEEE Trans. Electromagn. Compat.*, vol. 58, no. 3, pp. 747–757, 2016.

[9] A. Fallahi and A. Enayati, "Modeling Pyramidal Absorbers Using the Fourier Modal Method and the Mode Matching Technique," *IEEE Trans. Electromagn. Compat.*, vol. 58, no. 3, pp. 820–827, Jun. 2016.

[10] A. K. Singh, M. P. Abegaonkar, and S. K. Koul, "Dual- and Triple-Band Polarization Insensitive Ultrathin Conformal Metamaterial Absorbers With Wide Angular Stability," *IEEE Trans. Electromagn. Compat.*, vol. 61, no. 3, pp. 878–886, Jun. 2019.

[11] M. A. Shukoor, S. Dey, and S. K. Koul, "A Simple Polarization-Insensitive and Wide Angular Stable Circular Ring Based Undeca-Band Absorber for EMI/EMC Applications," *IEEE Trans. Electromagn. Compat.*, vol. 63, no. 4, pp. 1025–1034, 2021.

[12] A. Kazemzadeh and A. Karlsson, "Multilayered wideband absorbers for oblique angle of incidence," *IEEE Trans. Antennas Propag.*, vol. 58, no. 11, pp. 3637–3646, 2010.

[13] B. A. Munk, P. Munk, and J. Pryor, "On designing Jaumann and circuit analog absorbers (CA absorbers) for oblique angle of incidence," *IEEE Trans. Antennas Propag.*, vol. 55, no. 1, pp. 186–193, 2007.

[14] J. Wang, R. Yang, J. Tian, X. Chen, and W. Zhang, "A Dual-Band Absorber with Wide-Angle and Polarization Insensitivity," *IEEE Antennas Wirel. Propag. Lett.*, vol. 17, no. 7, pp. 1242–1246, 2018.

[15] O. Luukkonen, F. Costa, C. R. Simovski, A. Monorchio, and S. A. Tretyakov, "A thin electromagnetic absorber for wide incidence angles and both polarizations," *IEEE Trans. Antennas Propag.*, vol. 57, no. 10 PART 2, pp. 3119–3125, 2009.

[16] Y. Cheng, H. Yang, Z. Cheng, and N. Wu, "Perfect metamaterial absorber based on a split-ring-cross resonator," *Appl. Phys. A Mater. Sci. Process.*, vol. 102, no. 1, pp. 99–103, 2011.

[17] C. Y. Lu, C. C. Chung, T. J. Yen, and T. Y. Huang, "Achieving broad absorption band and high incident angles by stochastically-distributed oblique-flat-sheet metamaterial perfect absorbers," *Sci. Rep.*, vol. 11, no. 1, 2021.

[18] Y. Shen, Y. Pang, J. Wang, H. Ma, Z. Pei, and S. Qu, "Origami-inspired metamaterial absorbers for improving the larger-incident angle absorption," *J. Phys. D. Appl. Phys.*, vol. 48, no. 44, 2015.

[19] T. Shi *et al.*, "Near-Omnidirectional Broadband Metamaterial Absorber for TM-Polarized Wave Based on Radiation Pattern Synthesis," *IEEE Trans. Antennas Propag.*, vol. 70, no. 1, pp. 420-429, 2022.

[20] X. Q. Lin, P. Mei, P. C. Zhang, Z. Z. D. Chen, and Y. Fan, "Development of a Resistor-Loaded Ultrawideband Absorber with Antenna Reciprocity," *IEEE Trans. Antennas Propag.*, vol. 64, no. 11, pp. 4910–4913, 2016.

[21] Y. Cai, X. Q. Lin, J. W. Yu, and S. Zhang, "Design of an absorber for large incident angles with antenna reciprocity," *2019 Photonics Electromagn. Res. Symp. - Fall, PIERS - Fall 2019 - Proc.*, pp. 521–524, 2019.

[22] T. R. Cameron and G. V. Eleftheriades, "Analysis and Characterization of a Wide-Angle Impedance Matching Metasurface for Dipole Phased Arrays," *IEEE Trans. Antennas Propag.*, vol. 63, no. 9, pp. 3928–3938, 2015.

[23] Y. H. Lv, X. Ding, B. Z. Wang, and D. E. Anagnostou, "Scanning Range Expansion of Planar Phased Arrays Using Metasurfaces," *IEEE Trans. Antennas Propag.*, vol. 68, no. 3, pp. 1402–1410, 2020.

[24] B. A. Munk, "Finite Antenna Arrays and FSS," *Finite Antenna Arrays FSS*, 2005.

[25] L. Zhang, H. Lu, P. Zhou, J. Xie, and L. Deng, "Oblique Incidence Performance of Microwave Absorbers Based on Magnetic Polymer Composites," *IEEE Trans. Magn.*, vol. 51, no. 11, 2015.

[26] R. Bansal, "Antenna theory; analysis and design," *Proc. IEEE*, vol. 72, no. 7, pp. 989–990, 2008.

[27] P. Mei, X. Q. Lin, G. F. Pedersen, and S. Zhang, "Design of a Triple-Band Shared-Aperture Antenna With High Figures of Merit," *IEEE Trans. Antennas Propag.*, vol. 69, no. 12, pp. 8884–8889, Dec. 2021.